High-speed tensile test instrument

P. H. Mott,[a] J. N. Twigg, and D. F. Roland
Chemistry Division, U. S. Naval Research Laboratory, Washington, DC 20375

H. S. Schrader
Science Applications International Corporation, La Plata, Maryland 20646

J. A. Pathak
Chemistry Department, George Mason University, Fairfax, Virginia 22030
and Chemistry Division, U. S. Naval Research Laboratory, Washington, DC 20375

C. M. Roland[b]
Chemistry Division, U. S. Naval Research Laboratory, Washington, DC 20375

(Received 29 September 2006; accepted 27 February 2007; published online 17 April 2007)

A novel high-speed tensile test instrument is described, capable of measuring the mechanical response of elastomers at strain rates ranging from 10 to 1600 s^{-1} for strains through failure. The device employs a drop weight that engages levers to stretch a sample on a horizontal track. To improve dynamic equilibrium, a common problem in high speed testing, equal and opposite loading was applied to each end of the sample. Demonstrative results are reported for two elastomers at strain rates to 588 s^{-1} with maximum strains of 4.3. At the higher strain rates, there is a substantial inertial contribution to the measured force, an effect unaccounted for in prior works using the drop weight technique. The strain rates were essentially constant over most of the strain range and fill a three-decade gap in the data from existing methods. © *2007 American Institute of Physics.*
[DOI: 10.1063/1.2719643]

I. INTRODUCTION

The stress-strain response of polymeric materials to high strains (~10) at high strain rates (up to 10^4 s^{-1}) is an unexplored area of behavior. This regime governs the performance of elastomers in various high-speed applications, such as skidding tires, rubber catapults and coatings for impact resistance and acoustic damping.[1] The performance in such applications often depends on the details of the stress-strain response, which for polymers depends strongly on strain rate.

A number of devices have been developed for measuring the mechanical response of polymers at high speed, but many do not allow visual observation of specimen deformation and failure. Other devices, such as the split Hopkinson pressure bar,[2,3] are limited in the range of strain that can be applied. In distinction, the tensile impact instrument described herein provides uniform, uniaxial deformation at an essentially fixed strain rate, with the entire experiment captured on video.

Previously various methods have been explored for measurement of the mechanical response of elastomers at high strain rates. Albertoni[4] modified a pendulum hammer to stretch a ring-shaped test piece to a predetermined elongation at constant strain rates up to ~40 s^{-1}. Following release of the rubber sample at the bottom of its fall, the pendulum continues to a new height, as determined by the retained energy. The difference in the initial and follow-through heights of the pendulum yields the energy to deform the sample. A different test specimen was used for each point on the obtained stress/extension curve. Roth and Holt[5] designed the first instrument to use a falling weight, achieving strain rates up to 20 s^{-1}. A ring-shaped specimen was stretched at a rate that initially increased, then decreased. Villars[6] achieved strain rates as high as 2700 s^{-1} with a device employing a spinning wheel. A pin on the edge of the wheel strikes a rubber sample in the form of a loop, stretching it at a constant rate. A piezoelectric crystal was used to measure the force. Compressive strain rates approaching 200 s^{-1} were achieved by Gale and Mills[7] with a falling weight apparatus. Integration of accelerometers attached to the weight was used to determine both the force and displacement of foam test samples. Hoge and coworkers[8,9] obtained high speed stress/strain measurements on a polystyrene foam using compressed gas to rapidly expand a piston and thereby stretch the sample at rates up to 100 s^{-1}.

The instrument most commonly used to measure high-speed mechanical behavior is the split Hopkinson bar, originally developed for steel but since applied to other materials, including polymers.[2,3,10] A sample is placed between two long elastic bars, typically aluminum. A third, smaller "striker" bar is accelerated toward the incident bar. The reflected and transmitted pulses are measured, usually with strain gauges attached to the bars, and from these the properties of the sample are deduced. The requirement of dynamic stress uniformity limits the maximum deflection and minimum strain rate.[11] In soft materials, the minimum reported strain rate is high, ~650 s^{-1} in compression and 800 s^{-1} in tension, with maximum strains of only 0.12 and

[a]Electronic mail: peter.mott@nrl.navy.mil
[b]Electronic mail: mike.roland@nrl.navy.mil

0.25, respectively.[12,13] The recent development of pulse shaping methods provides nearly constant strain rates to moderate strains.[14] For elastomers, spatially homogeneous uniaxial compression is difficult to achieve due to the tendency of these materials to adhere to the loading surface. This adhesion causes subtle "bulging," indicative of mixed modes of deformation (i.e., compression in the central region and shear at the interfaces). For thin cylinders this "barreling" necessitates a large correction of the measured data.[15–17] Verification of truly flat cylindrical surfaces is complicated by the tradeoff between time and spatial resolution in the imaging of high speed measurements.[12]

The instrument described herein is a modification of an existing design by Hoo Fatt and co-workers.[18–20] In their device the impact energy is supplied by a Charpy-type pendulum, which contacts a slider bar that pulls directly on cables attached to shuttles; sample grips are attached to the latter. The speed of the slider bar is equal to the tangent velocity of the pendulum, so that the velocity of the cables is determined by the drop-height of the pendulum and the angle between the cables and the slider bar. With such an arrangement, the shuttle speed is less than the pendulum speed.

II. DESCRIPTION

Figure 1 shows a schematic of the present device, which is adapted from an MTS impact tester. A 100 kg drop weight is raised on a vertical track to a given height and then released. Attached to the bottom of the weight are two round impact bars. Extending forward, these bars engage L levers, which pivot about bearings as the drop weight falls, to pull attached cables. The cables pass around pulleys and are attached to shuttles, which are in turn caused to move in opposite directions on linear bearings on a horizontal track. The tensile force is measured by load cells at each end of the sample.

A high speed digital camera (Vision Research Phantom 7 monochrome) records the motion, with the positions of fiducial marks, on both the shuttles and the sample, determined by image analysis (Image Express Motion Plus). The 704 $\times$96 pixel images are recorded in 12-bit resolution. Strain in the dumbbell-shaped sample (conforming to ASTM D4482[21] and shown in Fig. 1) are determined by the change in length between marks at either end of the test section; thus, end effects are avoided.

Typical motion of the (empty) shuttles is shown in Fig. 2. For equilibrium (zero net acceleration of the sample), it is necessary that the forces applied at both ends of the sample remain equal throughout the measurement. This is accomplished by attention to symmetry: the L levers must be the same distance from the impact bars (adjusted using shims), at the same angle to the vertical (adjusted using stops), and centered between the impact bars (adjusted by moving the base). Figure 2 shows that the difference between the start of the shuttle movements, as determined by fitting the sample speed to Eq. (1) (see Sec. III), was less than 1 ms, with the shuttle speeds differing by no more than 0.2 m/s at the conclusion of the test. This is a typical result and experiments that exceeded these differences are discarded. Shuttle speeds

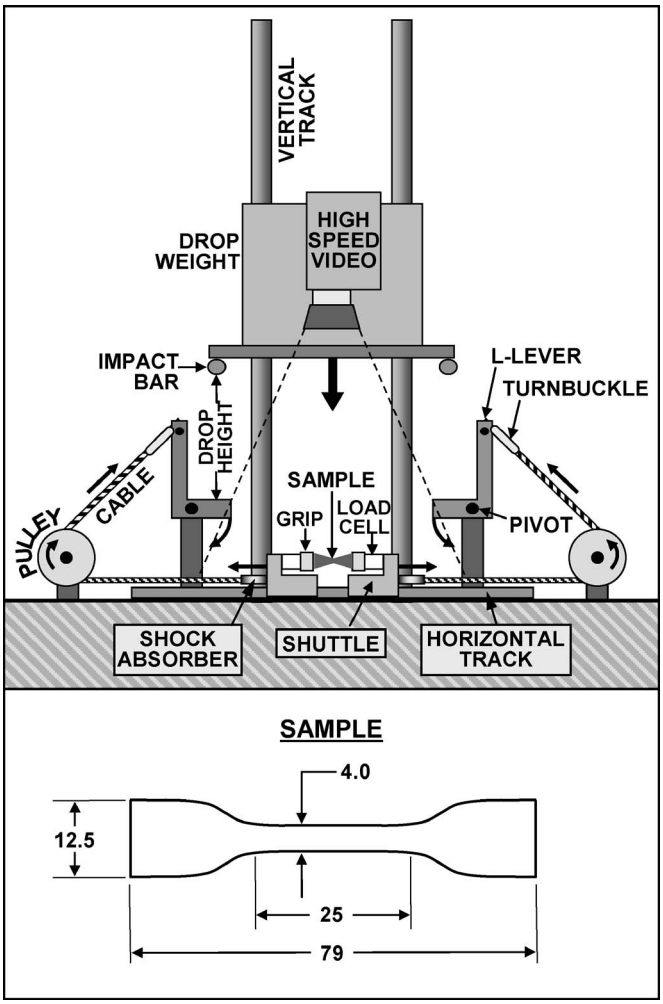

FIG. 1. Top: schematic of the high-speed tensile test machine. Bottom: ASTM 4482 sample geometry (dimensions in mm). Sample thickness is 1.5 mm.

herein ranged from 4 to 10 m/s, depending on the drop height. Using the maximum available height, shuttle speeds of $\sim$26 m/s can be achieved.

Small shock absorbers were fitted in the loading train

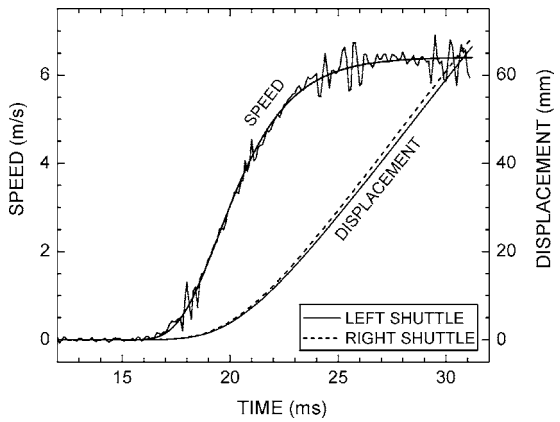

FIG. 2. Shuttle displacement and speed from a 0.229 m drop height without a sample present. The left shuttle speed was found by numerical differentiation; the right shuttle speed was indistinguishable from the left and has been omitted for clarity. The smooth line is the fit to the shuttle speed from Eq. (1), with s_M=6.41 m/s, t_0=9.26 ms, and k=538.8 s^{-1}.

near the shuttles to damp out vibrations occurring during the first 2–3 ms. These were fabricated from 50 mm long nylon-reinforced PVC tubing mounted on barbed brass fittings. During the impact, the tubing stretched markedly, damping out high frequency spikes in the measured load. The cables were kept taut by a light tension spring stretched between the shuttles (not shown in Fig. 1 for clarity). If the shock absorbers are omitted, the force and accelerometer data become much noisier.

Two different load cells were employed: for slow measurements a conventional, strain-gauge type load cell (Futek LCM300), and for fast measurements a piezoelectric load cell (PCB Piezotronics, Inc., Link ICP quartz force sensor). The latter self-discharges too quickly (half-life ~9.4 s) for low strain rate experiments. Turnbuckles are adjusted to zero the initial force on the unstrained sample. Accelerometers (PCB Piezotronics, Inc., quartz shear ICP accelerometer) were also attached to the shuttles. Load cell calibration was carried out at low speed, using the winch motor, with a steel spring mounted between the shuttles. The force-deflection results were compared to data from measurements with an Instron 5500R.

The load cell and accelerometer signals were recorded simultaneously at 10^4 Hz with an analog-to-digital (A/D) system external to the data computer (National Instruments, Inc., high-speed data acquisition system). A signal from a photoelectric sensor (Automatic Timing & Controls 7703A) simultaneously triggered the A/D system and the digital camera, which are operated at the same rate (10^4 frames/s) to simplify data analysis. Timing between the two devices was established by comparing the inertial peak force (see Sec. III) to the maximum acceleration of the shuttle; it was found that the A/D system inserted a 0.3 ms delay to the data. A comparison of the force and frame index at sample failure, which typically occurs ~30 ms after the trigger, verified that the A/D and digital camera acquisition rates were equal within the precision of the measurement.

To illustrate the instrument performance, two rubbers were tested, a nitrile rubber[22] and a commercial polyurea (Dow Chemical Isonate 143L and Air Products Versalink P1000, 1:4 stoichiometry). Both are high modulus elastomers with substantial toughness. The nitrile rubber was mixed in a two roll laboratory mill and then compression molded into sheets, first at 125 °C for 30 min, and then at 160 °C for 35 min. The polyurea was degassed with an internal mixer, and then sprayed into sheets for curing at room temperature. Test samples from both materials were die cut from the molded sheets.

III. INERTIA CORRECTION

In conventional stress-strain test measurements, the highest displacement rate does not exceed about 0.01 m/s, with corresponding strain rates of ~0.1 s^{-1}. Inertial forces in such measurements can be neglected since they are smaller than other sources of error (e.g., load cell drift due to temperature fluctuations). In the high rate measurements discussed herein, however, the inertial force can be substantial, so it must be subtracted from the total force.

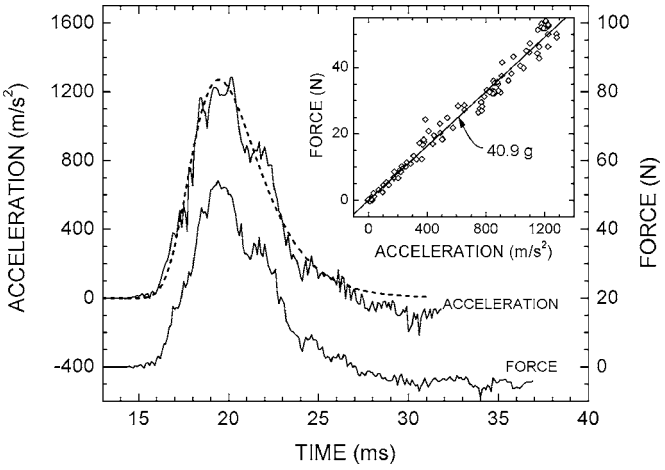

FIG. 3. Comparison of the accelerometer and load data (no sample) from the same measurement as Fig. 2. The smooth line is from derivative [Eq. (3)] of the fit to the shuttle speed. The inset plots the force as a function of the accelerometer data; the indicated slope is the effective mass of the load cell and grips.

To quantify the inertia, tests were carried out with no sample in place. The shuttle speed s was determined by numerical derivative of the displacement, as shown in Fig. 2. These data were fit to the Gompertz growth curve[23]

$$s = s_M \exp\{-\exp[-k(t-t_0)]\}, \tag{1}$$

where s_M is the maximum speed, t_0 is the offset time, and k is the sharpness of the S-shaped inflection. This expression was chosen for its simplicity and fidelity to the data; Fig. 2 shows the agreement with the measurement. The shuttle acceleration a was then found from the derivative

$$a = s_M k \exp\{-k(t-t_0) - \exp[-k(t-t_0)]\}. \tag{2}$$

Figure 3 shows the force from the piezoelectric load cell, the output of the accelerometer, and the acceleration determined from the derivative of the shuttle speed, all plotted as a function of time. The agreement between these data and the fit of Eq. (2) is excellent, verifying the accelerometer calibration.

The force F in Fig. 3 is the result of the acceleration a of the grips and other hardware attached to the sensing end of the load cell; the two quantities are related by[24]

$$F = ma, \tag{3}$$

where m is the effective mass of the grip hardware. Comparing the positions of the small fluctuations in the accelerometer and force data, it is clear that these features reflect genuine changes in the movement of the shuttles, not artifacts due to noise. It is also evident that the accelerometer is more faithful to the shuttle acceleration than the fit to the image analysis data. At times beyond 27 ms, both the force and the accelerometer are slightly negative, indicating that the shuttle is slowing. This behavior is difficult to discern, given the scatter in the shuttle speed data in Fig. 2, nor is it captured by the fit using Eq. (1). The inset in Fig. 3 shows the measured force as a function of the accelerometer response; these data are linear, passing through the origin with a slope equal to the effective mass.

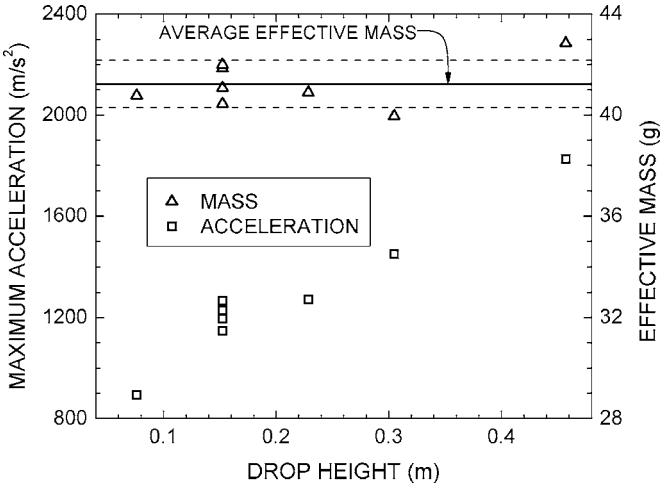

FIG. 4. Summary of inertia effect with the grip hardware attached for the piezoelectric load cell. Dashed lines show one standard deviation.

This mass, along with the maximum acceleration [from Eq. (2)], are displayed as a function of drop height in Fig. 4. The maximum acceleration varies from 893 to 1826 m/s^2, with the effective mass found to be constant, equal to 41.2 ± 0.9 g (the error is one standard deviation). This mass reflects the weight of the grip, stud, and two jam nuts, plus the intrinsic (internal) inertia of the piezoelectric load cell. Similar measurements carried out after removal of the detachable hardware yielded an effective mass of 18.94 ± 1.2 g. The difference, 22.3 g, compares well with the actual weight of the grip hardware, 20.24 g. For comparison, the sample weight was typically ~1.5 g.

A similar set of measurements was carried out for the other shuttle, fitted with the conventional load cell. The effective mass was 11.8 g, which was reduced by 9.6 g with all hardware removed. This compares well to the actual weight of the hardware, 9.4 g. The lower mass of this shuttle is due to differences in configuration.

IV. STRAIN

Figure 5 shows a sequence of four digital photographs taken during a test of the nitrile rubber. The marks x_1 and x_2 identify the ends of the (uniform) sample gauge length and S_1 and S_2 identify the grip positions. The images at 3.3 and 6.3 ms show that the gauge length region is deforming uniformly, without propagating waves. Interestingly, at 6.3 ms the gauge length has changed to a "white" color (in the black and white image). In other stress-strain measurements, carried out at a strain rate of 0.1 s, the rubber also turned white at large strain; the cause is unknown. The failure of the specimen at 8.0 ms shows a small portion to be unloaded. Since the failure occurred in the uniformly strained test region, the failure strain and stress can be determined.

A comparison of the engineering strain measured in two different ways is shown in Fig. 6. The ordinate is the apparent strain, determined from the displacement of the sample grips (S_1 and S_2 in Fig. 5) normalized by the gauge length (L_0 in Fig. 5). The abscissa represents the actual strain, obtained from the displacement of the points at the end of the gauge length (x_1 and x_2 in Fig. 5) normalized by L_0. The apparent strain overestimates the actual strain by a factor of 2. The apparent strain rate would have the same error; thus, strain rates reported from shuttle displacements overestimate the strain rate,[18] by an amount depending on the sample shape.

Immediately after the sample fails (at 8.0 ms, in the bottom photograph of Fig. 5), the specimen retracts after an unloading wave passes through the length of the sample.[25]

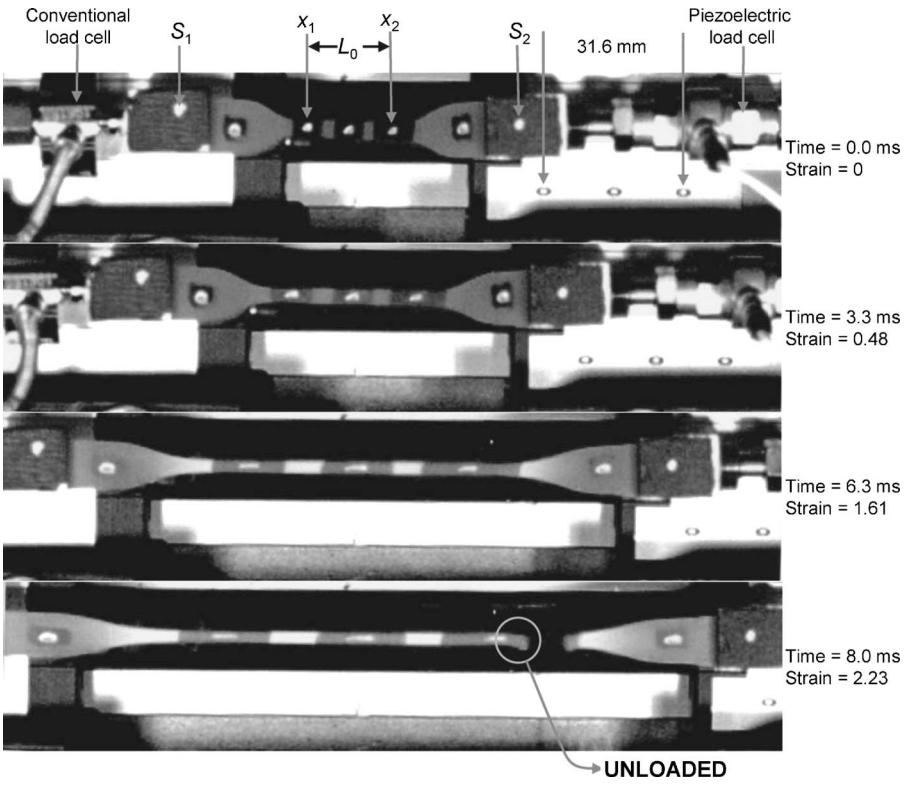

FIG. 5. Sequence of four photographs of the nitrile rubber for a drop height of 0.61 m (strain rate =360 s^{-1}).

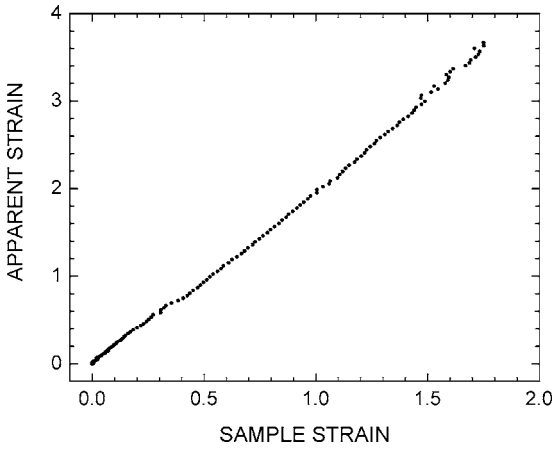

FIG. 6. Comparison of apparent strain, found by the relative displacement of points S_1 and S_2 in Fig. 5, to the actual strain, found by the relative displacement of points x_1 and x_2.

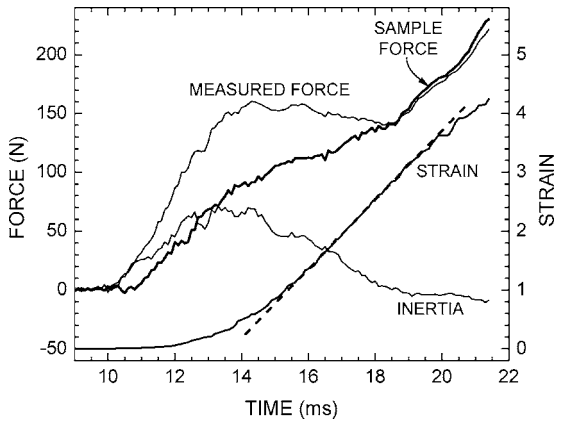

FIG. 7. Forces from the piezoelectric load cell, deduced from the accelerometer (inertia) and calculated for the polyurea sample with a 0.61 m drop height. The strain was obtained from the camera images. Note the offset between the strain and the load scales. The dashed line shows the range of constant strain rate; its slope is 588 s^{-1}.

The unloading wave moves as a pulse at a constant speed v_u, determined in separate experiments to be 1001 ± 72 and 320 ± 20 m/s at 100% strain for the nitrile and polyurea compounds, respectively.[26] The unloading wave is isochorically constrained to one dimension, and is different from a longitudinal wave that occurs in three dimensions with volumetric strain. The unloading wave speed is

$$v_u = (1+e)\left(\frac{E}{\rho}\right)^{1/2}, \tag{4}$$

where e is the engineering strain, E is Young's modulus, and ρ is the density.[27–29] The one-dimensional unloading wave speed is sensitive to the strain, and is approximately 1/50 of the more familiar longitudinal wave speed. After the unloading wave passes, the unloaded rubber undergoes strain recovery at a slower rate that depends on the viscoelastic response of the polymer. Assuming that a loading pulse is identical to an unloading pulse, the speed of the unloading wave establishes both the maximum strain rate that can be achieved in a dynamically homogeneous measurement and also the time resolution. The maximum strain rate is

$$\dot{\bar{\varepsilon}}_{\max} = \frac{v_u}{L_{\text{tot}}}, \tag{5}$$

where L_{tot} is the total distance the unloading wave must travel (=1/2 the distance between the grips, or approximately 30 mm). Thus, the maximum strain rate is ~33 000 and 10 700 s^{-1} for the nitrile rubber and polyurea, respectively. These values are 1.5–2 orders of magnitude greater than the strain rates attained herein. The time resolution, or time required for a pulse to travel down the sample, is just the reciprocal of Eq. (5), and equal to 0.03 and 0.09 ms for the nitrile rubber and polyurea, respectively. Data taken over such time intervals, or taken at deflection rates approaching the loading wave speed, reflect a transitory wave and are therefore not kinematical. The tensile behavior of an elastomer tested at speeds greater than the loading wave is predicted to be either a rarefaction wave or a shock, or a combination of the two.[30]

V. STRESS-STRAIN CURVES

The forces measured by the piezoelectric load cell and the inertial forces from accelerometer data are displayed in Fig. 7, for the polyurea using a 0.61 m drop height. The inertial force was found from the product of the acceleration and the separately measured effective inertial mass (described earlier); the sample force was found by subtracting the inertial force from the measured load. Over the first 0.8 ms, from the start at 10 ms until 10.8 ms, inertia accounts for nearly all of the force, consequently delaying the start of the sample loading. Inertia continues to contribute significantly though 18.7 ms. Afterward, the inertial force is negative due to a small deceleration of the shuttle and from this point onward the sample load slightly exceeds the measured force.

Figure 7 shows that the strain is also delayed from the start by about 0.8 ms. It smoothly accelerates up to a strain of 1.13 at 15.6 ms, whereupon it becomes linear. Beginning at a strain of 3.26 at 1.92 ms, there is slight deceleration. The strain rate in the linear region was 588 s^{-1}.

The resulting engineering stress-strain curve from this measurement is shown in Fig. 8. This figure compares the sample forces (inertia corrected) from each load cell, normalized by the original cross-sectional area. The two curves are in agreement within the scatter. The fact that the forces at each end are equal confirms the absence of acceleration of the sample. For comparison, Fig. 8 also displays the stress-strain behavior measured with an Instron machine at a much lower strain rate. This curve is lower due to greater relaxation of the polyurea during the loading.

Engineering stress-strain curves for the nitrile rubber at varying strain rates are displayed in Fig. 9. The curves for the higher strain rates show the stress increasing with strain rate. Interestingly, the curve for 0.008 s^{-1} crosses the curve for 166 s^{-1}, at a strain of 2.45; the reason for this is unknown (the elastomer is a random copolymer and thus not expected to crystallize). One possible difference is nonisothermal conditions for the adiabatic high strain rate test. Comparing Fig. 8 to Fig. 9, the nitrile rubber is much stiffer than the poly-

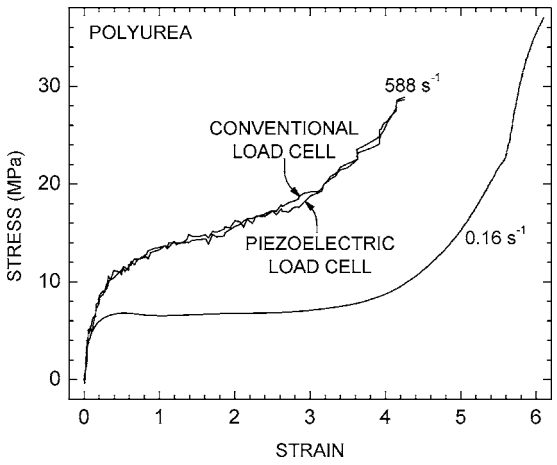

FIG. 8. Stress-strain curve from the polyurea measurement in Fig. 7. The nominal strain rate of 588 s^{-1} occurred over strains from 1.1 to 3.2. Also included is the stress-strain curve of the polyurea measured with a conventional test machine (Instron) at the indicated strain rate.

urea; consequently, for a given drop height, the strain rate in the nitrile rubber was somewhat lower (and ν_u higher).

VI. ADVANTAGES AND LIMITATIONS

The device described herein is an improvement over a previous, somewhat similar instrument.[19] Referring to Fig. 1, the vertical track with a free-falling weight and the use of L levers are significant enhancements. These increase both the maximum available shuttle speeds and the maximum displacement. The strain rate is essentially constant over a substantial portion of the stress-strain curve. The use of a dogbone-shaped sample together with high speed imaging enables accurate strain measurement, as well as the determination of the strain and stress at failure. The inclusion of accelerometers on the shuttles permits inertia to be measured and subtracted from the stress/strain curves. The difference between the measured and the sample forces (Fig. 7) shows the significance of this correction.

The minimum and maximum available strain rates for this instrument are governed by practical considerations and have not been fully explored. The lowest strain rate to date, 14 s^{-1}, was achieved using a winch motor to lower the weight. Of course, using a sample with a longer test section, anchoring one of the shuttles, and other minor modifications can be employed to decrease this by a factor on the order of 10, which would approach the strain rate of conventional (e.g., screw-driven) instruments. The highest strain rate reported herein, 588 s^{-1} (Figs. 7 and 8), corresponds to a 0.61 m drop height. The maximum drop height with our configuration is 4.57 m. Since the speed of the falling weight is [Eq. (3)]

$$s_W = (2gh)^{1/2}, \tag{6}$$

where g is the acceleration due to gravity (9.81 m/s) and h is the drop-height, the maximum strain rate is about 1600 s^{-1}. The shock absorbers, used to reduce vibrations at the onset of a test, reduce the actual shuttle speeds. Also, as the speed is increased, the shuttle acceleration occurs over a larger portion of the test, reducing the range of constant strain. These limitations may be overcome to some extent by modifying the geometry of the sample, the shock absorbers, and the L levers.

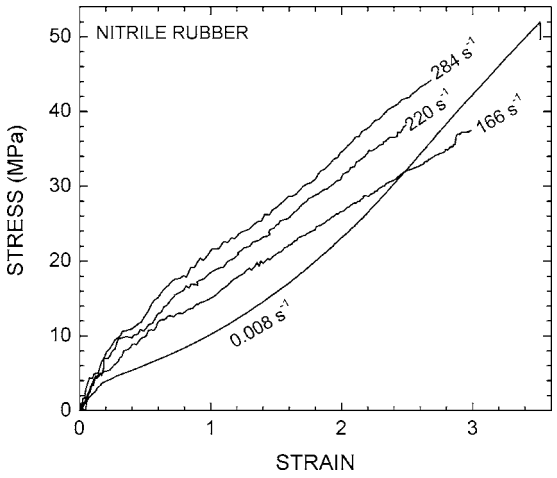

FIG. 9. Stress-strain curves of nitrile rubber at the indicated nominal strain rates. The curve at a strain rate of 0.0088 s^{-1} was measured with an Instron.

ACKNOWLEDGMENTS

The authors are grateful to L. Levenberry for engineering work, D. P. Owen for preparing the polyurea films, and R. Bogoslovov for helpful discussions. This work was supported by the Office of Naval Research.

[1] C. M. Roland, Rubber Chem. Technol. **79**, 429 (2006).
[2] B. Hopkinson, Philos. Trans. R. Soc. London, Ser. A **213**, 437 (1914).
[3] H. Kolsky, Proc. Phys. Soc. London, Sect. B **62**, 676 (1949).
[4] G. J. Albertoni, Rubber Chem. Technol. **10**, 317 (1937).
[5] F. L. Roth and W. L. Holt, Rubber Chem. Technol. **13**, 348 (1940).
[6] D. S. Villars, J. Appl. Phys. **21**, 565 (1950).
[7] A. Gale and N. J. Mills, Plast. Rubber Process. Applic. **5**, 101 (1985).
[8] K. G. Hoge and R. J. Wasley, J. Appl. Polym. Sci.: Appl. Polym. Symp. **12**, 97 (1969).
[9] J. A. Rinde and K. G. Hoge, J. Appl. Polym. Sci. **15**, 1377 (1971).
[10] J. Yi, M. C. Boyce, G. F. Lee, and E. Balizer, Polymer **47**, 319 (2006).
[11] L. M. Yang and V. P. W. Shim, Int. J. Impact Eng. **31**, 129 (2005).
[12] B. Song and W. Chen, J. Eng. Mater. Technol. **125**, 294 (2003).
[13] P. J. Rae and E. N. Brown, Polymer **46**, 8128 (2005).
[14] W. Chen, B. Zhang, and M. J. Forrestal, Exp. Mech. **39**, 81 (1999).
[15] A. N. Gent and P. B. Lindley, Proc. Inst. Mech. Eng. **173**, 111 (1959).
[16] P. H. Mott and C. M. Roland, Rubber Chem. Technol. **68**, 739 (1995).
[17] M. L. Anderson, P. H. Mott, and C. M. Roland, Rubber Chem. Technol. **77**, 293 (2004).
[18] I. Bekar, M. S. Hoo Fatt, and J. Padovan, Tire Sci. Technol. **30**, 45 (2002).
[19] M. S. Hoo Fatt, I. Bekar, and J. Padovan, U. S. Patent application No. 20040040369, 2003.
[20] M. S. Hoo Fatt and I. Bekar, J. Mater. Sci. **39**, 6885 (2004).
[21] ASTM 4482, "*Rubber property-extension cycling fatigue*" (ASTM International, West Conshohocken, PA).
[22] I. S. Choi, C. M. Roland, and L. C. Bissonnette, Rubber Chem. Technol. **67**, 892 (1994).
[23] B. Gompertz, Philos. Trans. R. Soc. London **123**, 513 (1825).
[24] J. S. Newton, *Philosophiæ Naturalis Principia Mathematica* (Samuel Pepys, London, 1687).
[25] P. Mason, Proc. R. Soc. London, Ser. A **272**, 315 (1963).
[26] R. Bogoslovov and C. M. Roland (unpublished).
[27] A. N. Gent and P. Marteny, J. Appl. Phys. **53**, 6069 (1982).
[28] H. M. James and E. Guth, Phys. Rev. **66**, 33 (1944).
[29] B. A. Mrowca, S. L. Dart, and E. Guth, J. Appl. Phys. **16**, 8 (1945).
[30] J. K. Knowles, J. Appl. Math. **62**, 1153 (2002).